Gas Absorption Studies in Microporous Hollow Fiber Membrane Modules

Sujatha Karoor[†] and Kamalesh K. Sirkar*

Department of Chemistry and Chemical Engineering, Stevens Institute of Technology, Castle Point, Hoboken, New Jersey 07030

A comprehensive experimental investigation of gas–liquid absorption in a shell-and-tube type microporous hydrophobic hollow fiber device in a parallel flow configuration was carried out. Two modes of countercurrent gas–liquid contacting were studied, the wetted mode (absorbent liquid filled pores) and the nonwetted mode (gas-filled pores). The absorbent flowed through the fiber bore in most of the experiments. The systems studied include pure CO_2, pure SO_2, CO_2–N_2 mixtures and SO_2–air mixtures. The absorbent was pure water. The absorption process was simulated for each case with a numerical model for species transport with and without chemical reaction. Laminar parabolic velocity profile was used for the tube-side flow, and Happel's free surface model was used to characterize the shell-side flow. The model simulations agreed well with the experimental observations in most cases. SO_2 removals as high as 99% were obtained in small compact contactors. High $K_L a$ and low height of transfer unit (HTU) values were obtained with hollow fiber contactors when compared to those of conventional contactors.

Introduction

In conventional large-scale gas absorption processes, the gas mixture is contacted with a scrubbing liquor in devices like packed towers, spray towers, venturi scrubbers, and bubble columns. These dispersion-based contacting methods have many drawbacks. An approach having much promise and without these shortcomings is membrane-based contacting using microporous hydrophobic hollow fibers. The microporous membrane-based device acts as a gas absorber, with the gas flowing on one side and the absorbent liquid flowing on the other side of the membrane without either phase being dispersed in the other. The gas–liquid interface is at the pore mouth. Unlike that in a true liquid membrane process, the absorbent liquid has to be regenerated in a separate stripper which can be also a membrane-based contactor.

A membrane-based contacting device can have a number of configurations. The focus here will be *primarily* on parallel flow modules of microporous hollow fibers. The membranes can be hydrophobic or hydrophilic, and the pores can be either gas filled or absorbent filled. The absorbent may flow on the tube side or shell side. These membrane-based gas separation devices offer several advantages over conventional contacting devices: much higher surface area per unit contactor volume; independent control of gas and liquid flow rates without any flooding, loading, weeping, or foaming; known gas–liquid interfacial area; modularity, easy to scale up or down; availability of all of the membrane surface area for contacting regardless of how low the individual phase flow rates are.

These advantages have led a number of investigators to xplore different applications. The first known application of a microporous membrane as a gas–liquid contacting device using hydrophobic flat Gore-Tex membranes of polytetrafluoroethylene was for oxygenation of blood (Esato and Eiseman, 1975). Tsuji et al. (1981) used hydrophobic microporous hollow fibers of polypropylene
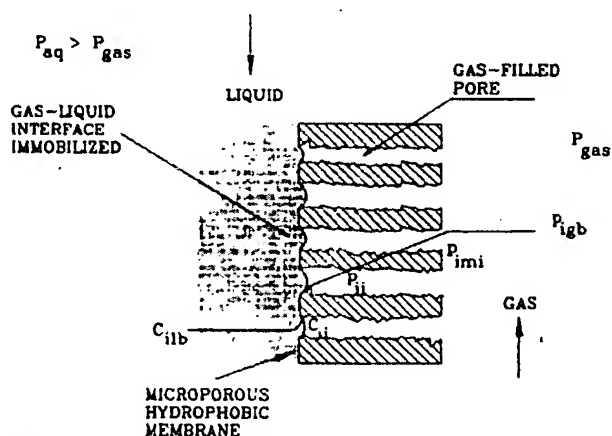
* To whom correspondence should be addressed. Current address: Department of Chemical Engineering, Chemistry and Environmental Science, New Jersey Institute of Technology, Newark, NJ 07102.

† Current address: Department of Chemical Engineering, MIT, Cambridge, MA 02139.
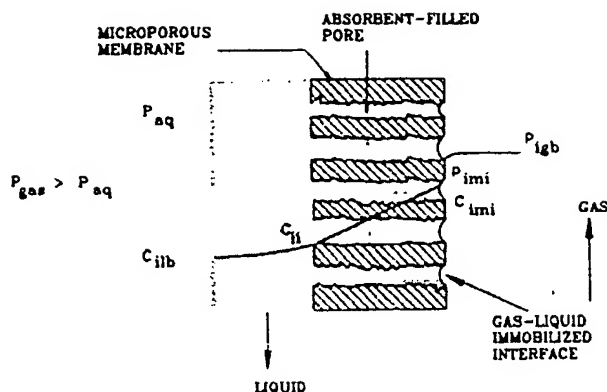
Figure 1. Nonwetted mode of hydrophobic membrane-based gas–liquid contacting.

for blood oxygenation. The applications of direct interest here are those for acid gas cleanup. Qi and Cussler (1985a,b) studied the absorption of a number of gases using various solvents and aqueous solutions in a hydrophobic microporous hollow fiber device where the membrane pores were gas filled. Yang and Cussler (1986) have noted a 10-fold increase in the gas separation efficiency when using a hollow fiber device over a conventional packed column. Ogundiran et al. (1988, 1989) in their experiments with absorption of SO_2 using microporous hydrophobic hollow fibers found this technique to be an extremely promising alternative to conventional scrubbers used for flue gas desulfurization. Sirkar (1992) has recently reviewed microporous membrane-based gas absorption processes.

The above-mentioned contacting studies were carried out using a microporous hydrophobic membrane. Figure 1 shows an absorbing liquid (that does not wet the fibers) flowing on one side and gas flowing on the other side. The gas pressure (P_{gas}) has to be lower than that of the liquid (P_{aq}) to prevent dispersion of gas as bubbles in the liquid. Liquid does not enter the pores unless a certain critical pressur is exceeded (Kim and Harriott, 1987). This mod of operation is identified as the nonwetted mode since the liquid does not wet the membrane and the membrane pores are gas filled. The gas/liquid interface shown in Figure

Figure 2. Wetted mode of membrane-based gas-liquid contacting.

1 lies at the pore mouth of the hydrophobic fiber on the absorbing liquid side. In this mode the gas species being separated diffuses first through the gas in the membrane pores before dissolving in the absorbent. Because the pores in the fibers are gas filled, the gas-phase mass-transfer coefficients are much higher than the liquid-side mass-transfer coefficients if no fast reaction is taking place or when the gas solubility is very low. Thus gas absorption is likely to occur without practically any increase in mass-transfer resistance due to the presence of the membrane.

There is yet another mode of operation where the membrane pores are absorbent liquid filled; this is called the wetted mode and is shown in Figure 2. Here a hydrophilic membrane is spontaneously wetted by the absorbing liquid which flows on one side, while the gas flows on the other side. In the case shown in Figure 2, the gas pressure has to be higher than the liquid pressure to prevent the liquid from dispersing as drops in the gas. A hydrophobic membrane can also be used in this mode using a nonwetting liquid by employing an exchange process (Bhave and Sirkar, 1986, 1987) which allows one to incorporate a nonwetting absorbing solution in the hydrophobic membrane pores. This mode may be useful when there is a very fast or instantaneous liquid-phase reaction and the gas resistance would be controlling the rate of transfer. The membrane-phase resistance may be eliminated in such a mode of operation. There is another reason for investigating such a mode. If long-term operation of a hydrophobic membrane leads to wetting of the pores, such a mode of operation may be adopted.

In this paper, the absorption of acid gases like SO_2 and CO_2 have been investigated using modules of microporous hydrophobic hollow fine fibers. Experiments have been carried out with both gas-filled membrane pores (nonwetted mode) and liquid-filled membrane pores (wetted mode) using pure gases and their mixtures, with different absorbing liquids flowing either on the tube side or on the shell side. This paper focuses on pure water as absorbent. A second paper will cover diethanolamine in water. Although the absorption of CO_2 in water is essentially physical, absorption of SO_2 in water is very strongly influenced by ionization so that there is reactive absorption. Gas absorption models have been developed on the basis f first principles to explain the observed separation and evaluate some commonly used correlations. The present analysis attempts to pr vide a fundamental basis for understanding aspects of this promising contacting technique. The experimental values of K_La and HTU btained here have been compared with those available in the literature. Gaseous systems investigated here include pure CO_2, pure SO_2, CO_2-N_2 mixtures, and SO_2-air mixtures.

Experimental Section

Micropor us hydroph bic Celgard X-20 and X-10 polypropylene h llow fibers made by Hoechst Celanese Corporation (SPD, Charlotte, NC) were used. Able to withstand air temperatures up to 75-80 °C, these fibers have an internal burst strength greater than 220 psi. Both fibers have a bubble p int pressure of 150 psi and a mean pore diameter f 0.03 μm. The characteristics of hollow fiber modules 1-4 fabricated in the laboratory and used here are provided in Table I. Module 2 has the highest area/volume.

The gas composition was measured by a Hewlett-Packard 5890A gas chromatograph using a thermal conductivity detector (TCD). The detector response was recorded by a digital reporting integrator 3393A (H.P., Paramus, NJ). A 10-port gas sampling valve was utilized (Sengupta et al., 1990). A two-column system based on a 6-ft × ⅛-in. Chromosorb 108 column (Chrompack Inc., Bridgewater, NJ) and a 10-ft × ⅛-in. molecular siev (Alltech Associates, Deerfield, IL) column was used. The column sequence was reversed after 1.9 min to separate O_2 and N_2 by the molecular sieve column. By this reversal CO_2, SO_2, and moisture did not enter the molecular sieve column thereby ensuring it a longer lifetime. Sampling was done continuously.

The liquid-phase concentrations were analyzed and used to compare the gas analysis via mass balances. In the cas of pure CO_2 if the change in gas flow rate was limited, concentrations based on the liquid phase were considered more reliable. For CO_2, liquid-phase-concentration measurements were made using a CO_2 electrode (Orion Model 94-02, Orion Research, Cambridge, MA). The measurement range of this electrode was 4.4-440 ppm CO_2 at a pH range of 4.8-5.2. Reproducibility was ±2%. Titration procedures were also used to cross-check the data (Betz, 1962). The concentrations measured by the electrode and the titration method were in agreement in the low rang 0-100 ppm. In higher concentration ranges, a different titration method was used (Snell and Hitton, 1966). In the case of SO_2, the method of analysis was based on the procedure described in *Standard Methods for the Examination of Water and Waste Water* (AWWA, 1965).

Figure 3 shows the experimental setup used for gas absorption studies. The gas mixture to be separated or the pure gas to be absorbed was passed through the modul either on the shell side or on the tube side, and th absorbing liquid flowed countercurrently through the absorber on the other side, separated from the gas by the membrane walls. The gas flow rate was controlled by an electronic mass flow transducer and a flow controller (Models 8100 and 8200; Matheson, East Rutherford, NJ). Pressure gauges at the module inlet and outlet indicated the gas pressures which varied between 0 and 14 psig depending on the mode of operation. The gas stream outlet concentration was measured by a gas chromatograph (GC), after which the gas was vented into the laboratory exhaust hood. A needle valve was used to control the liquid flow rate. The liquid flow rate was measured at the outlet of the membrane contactor at regular intervals. The backpressure regulator (BPR) was not needed when the membrane pores were gas filled; i.e., the system was operated in the n nwetted mod . Experimentally observed concentration change from the feed to the outlet f the module in the gas phase was used to determine the verall logarithmic mean based verall mass-transfer coefficient K_{Olm}, using the f llowing equation:

Table I. Characteristics of Hollow Fiber Modules Used in This Study

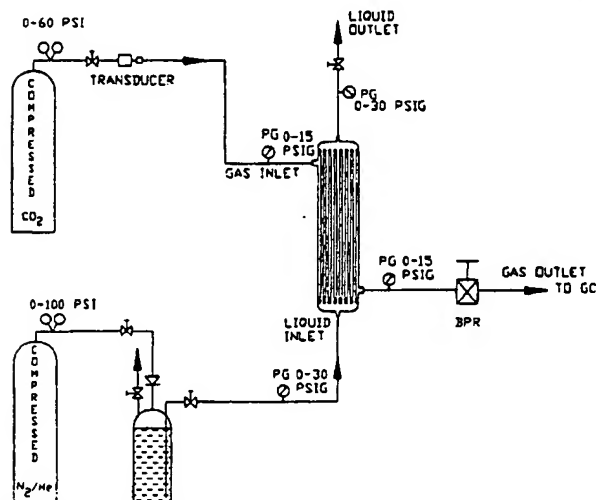| module no.	fiber o.d., μm	fiber i.d., μm	shell diam, cm	length of module, cm	no. of fibers	porosity	packing fraction	area of contact i.d., cm²	a, cm²/cm³
1	150	100	0.4572	30.0	102	0.2	0.1098	96.13	19.52
2	300	240	0.4927	30.0	132	0.4	0.4887	298.57	52.2
3	300	240	0.4572	18.0	75	0.4	0.3229	101.78	34.44
4	300	240	0.4572	17.5	75	0.4	0.1098	98.96	34.44

Figure 3. Gas absorption using hollow fibers: experimental setup.

$$K_{Olm} = \frac{V_l C_{l\,out}}{60 A_T \Delta C_{lm}} \qquad (1)$$

K_{Olm} is also denoted as K_L in this paper. A_T is based on the surface area of gas–liquid contact. The quantity ΔC_{lm}, the logarithmic mean concentration difference of gas species, is given by

$$\Delta C_{lm} = \frac{(HC_{g\,in} - C_{l\,out}) - (HC_{g\,out})}{\ln\left(\dfrac{HC_{g\,in} - C_{l\,out}}{HC_{g\,out}}\right)} \qquad (2)$$

Here H is Henry's law constant which is the ratio of the interfacial concentration of absorbed species i in liquid divided by that in the gas:

$$C_{il} = HC_{ig} = C_{Aw} \qquad (3)$$

if species i is represented by A and the liquid phase by w for water. In the case of CO_2–H_2O system, the value of Henry's law constant is 0.8314 at 25 °C (Geankoplis, 1972) and that for SO_2–H_2O is 25.86 at 25 °C (Hikita et al., 1978).

Model Development

A theoretical model is developed here to describe the absorption of pure CO_2, pure SO_2, and their mixtures in nitrogen or air by water. Both wetted and nonwetted modes of operation are considered here, and in both modes, the liquid flow was always countercurrent to the gas flow and on the tube side. The following assumptions were utilized: (1) steady state and isothermal condition; (2) no axial diffusion; (3) fully developed parabolic liquid velocity profile in the tube side; (4) use of Happel's free surface model (1959) to characterize the shell-size velocity profile; (5) ideal gas behavior; (6) applicability of Henry's law.

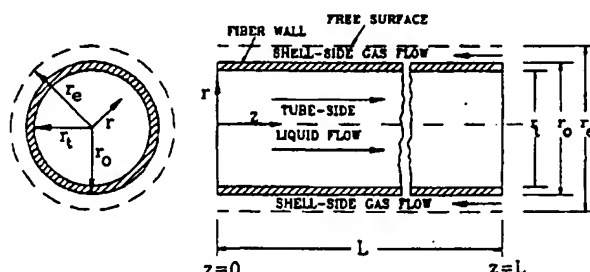Using these assumptions, the general f rm of the conservation equation for the absorption processes is given as

Figure 4. Free surface model (adapted from Gill and Bansal (1973)).

$$D_{ik}\left[\frac{\partial^2 C_{ijk}}{\partial r^2} + \frac{1}{r}\frac{\partial C_{ijk}}{\partial r}\right] = v_{zk}(r)\frac{\partial C_{ijk}}{\partial z} + (-r_i) \qquad (4)$$

In the above equation, i denotes the components involved (i = A, B, ...), j denotes the phase (gas (g), liquid (l)), and k denotes the location (shell (s), tube (t), or membrane (m)). The quantity v_{zk} is the prescribed axial velocity profile for the tube or the shell side. For the tube side a laminar parabolic velocity profile is assumed:

$$v_{zt} = 2\langle v_{zt}\rangle[1 - (r/r_t)^2] \qquad (5)$$

The flow in the shell side is usually very complex. Happel's (1959) free surface model as represented in Figure 4 is used to characterize the shell side velocity profile; it is given by the following equation:

$$v_{zs}(r) = 2\langle v_{zs}\rangle\left[1.0 - \left(\frac{r_0}{r_e}\right)^2\right] \times$$
$$\left[\frac{(r/r_e)^2 - (r_0/r_e)^2 + 2\ln(r_0/r)}{3 + (r_0/r_e)^4 - 4(r_0/r_e)^2 + 4\ln(r_0/r_e)}\right] \qquad (6)$$

where r_e is the radius of the free surface and is given as

$$r_e = \left[\frac{1}{1-\epsilon}\right]^{1/2} r_0$$

Pure Gas Absorption: Nonwetted mode. In this mode of absorption of pure CO_2, the pores of the membrane are filled with pure gas flowing in the shell side. There is no gas-phase-transport resistance. Due to the low value of the equilibrium constant (K_E = 4.4 × 10⁻⁷ mol/L), bicarbonate formation is neglected. Equations 4 and 5 are solved for the liquid phase for i = A = CO_2, j = l, k = t, and r_A = 0, along with the following boundary conditions. The concentration profile is symmetrical about the center of the tube and therefore satisfies

$$\frac{\partial C_{ilt}}{\partial r}(0,z) = 0 \qquad (7)$$

Further, since pure CO_2 gas of known pressure is present in the shell side, the species concentration at the inside wall ($r = r_t$), is known. Hence the boundary condition at the wall is
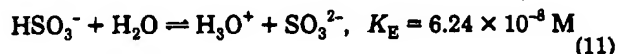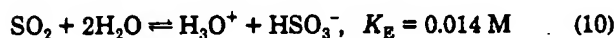
$$C_{ilt}(r_t,z) = C_{iw} \qquad (8)$$

Here C_{iw} is the product f Henry's law constant times gas-phase concentration and is given by eq 3. In most of the experiments conducted, the pure gas pressure remained

essentially constant along the module length. Therefore C_{iw} remained constant with z (which is essentially the Graetz solution (Skelland, 1974)). There were a few experimental situations where the pure gas pressure changed somewhat along the module. In such a case, C_{iw} varied with axial location z (linear variation was assumed for numerical calculations). The inlet condition is also known

$$C_{ilt}(r,0) = C_{inlet} = 0 \qquad (9)$$

So far in the species conservation equation, there was no reaction. The situation changes for absorption of pure SO_2 in water. The following hydrolysis reactions take place when SO_2 is absorbed in pure water:

$$SO_2 + 2H_2O \rightleftharpoons H_3O^+ + HSO_3^-, \quad K_E = 0.014 \text{ M} \qquad (10)$$

$$HSO_3^- + H_2O \rightleftharpoons H_3O^+ + SO_3^{2-}, \quad K_E = 6.24 \times 10^{-8} \text{ M} \qquad (11)$$

If the pH is less than 4–5, formation of SO_3^{2-} is negligible. By choosing operation conditions that exclude the pH range mentioned above, SO_3^{2-} formation is avoided (Seinfeld, 1980; Roberts, 1979). In the present study the operational conditions were such as to allow the assumption that only HSO_3^- formation is effective.

The diffusion coefficients of HSO_3^- (species B) and H_3O^+ at 25 °C are 1.47×10^{-5} and 9.3×10^{-5} cm^2/s, respectively. An electrical potential develops which retards the motion of H_3O^+ and speeds up HSO_3^-, so as to maintain electroneutrality. Thus an effective diffusion coefficient in the liquid is defined, which in the binary case is given as (Vinogard and McBain, 1941)

$$D_{Bl} = \frac{2D_{H_3O^+}D_{HSO_3^-}}{D_{H_3O^+} + D_{HSO_3^-}} \qquad (12)$$

The rate expressions for the reaction (eq 10), after using the electroneutrality condition, $C_{HSO_3^-} = C_{H_3O^+}$, are expressed by the following equations:

$$-r_{SO_2} = k_1 C_{SO_2} - \frac{k_1}{K_E}(C_{HSO_3^-})^2 \qquad (13)$$

$$-r_{HSO_3^-} = -k_1 C_{SO_2} + \frac{k_1}{K_E}(C_{HSO_3^-})^2 \qquad (14)$$

where the forward rate constant k_1 is given as 3.17×10^{-2} s^{-1} (Wang and Himmelblau, 1964). Since eq 4 is valid for both components SO_2 (A), and HSO_3^- (B), there are now two coupled partial differential equations to be solved along with the boundary conditions. With eqs 13 and 14 representing the reaction terms $-r_A$ and $-r_B$, respectively, eq 4 for SO_2 and eq 4 for HSO_3^- are solved simultaneously along with the above boundary conditions (eqs 7 and 8). In the case of HSO_3^- at the wall, equilibrium is assumed and the following equation is used to represent the wall condition:

$$C_{Blt}(r_t,z) = (C_{Aw}K_E)^{1/2} \qquad (15)$$

For details, see the thesis by Karoor (1992).

Wetted Mode. In this mode of operation the liquid is flowing in the tube and is also incorporated in the membrane pores. An additional equation is required to describe the diffusion through the membrane pores as the liquid-filled pores offer additional resistance. At high porosity (greater than 10%), Keller and Stein (1967) have shown that the diffusional process is essentially one dimensional. The following assumptions were made in deriving the membrane-phase equation:

1. The effective membrane-phase diffusion coefficient D_{im} is defined by $D_{il}\epsilon/\tau$.
2. The diameter of the pore is uniform.
3. There are no gradients in the direction normal to the pore axis.
4. There is no convective transport.

The species balance eq 4 is still valid for the liquid in the membrane phase ($j = 1, k = m$) for each species without the convection term. The following boundary conditions are used at the membrane–tube interface:

$$r = r_t, \qquad C_{ilm}|_{r_t} = C_{ilt}|_{r_t} \qquad (16)$$

A flux continuity at the same boundary is assumed, giving the equation

$$r = r_t, \qquad D_{im}\frac{\partial C_{ilm}}{\partial r}\Big|_{r_t} = D_{lt}\frac{\partial C_{ilt}}{\partial r}\Big|_{r_t} \qquad (17)$$

The equation for the membrane phase is solved using the above boundary conditions, namely eqs 16 and 17, to yield the following equation at the inner wall of the membrane $r = r_t$ (Karoor, 1992).

$$\frac{\partial C_{Alt}}{\partial r}\Big|_{r_t} = [C_{Alm}|_{r_0} - C_{Alt}|_{r_t}]\frac{D_{Am}}{D_{At}}\frac{1}{(\ln r_0 - \ln r_t)r_t} \qquad (18)$$

Now eq 4 for $i = A$, $j = 1$, and $k = t$ along with eq 18, the boundary condition eq 7, and the wall condition at $r = r_0$, $C_{ilm}(r_0,z) = C_{iw}$ are solved.

The above system of equations is for CO_2, since there is no reaction in the liquid phase. For SO_2, two species SO_2 (A) and HSO_3^- (B) are present and eq 4 is valid for each species for the tube side. The equations for the membrane phase are given as

$$D_{Am}\left[\frac{\partial^2 C_{Alm}}{\partial r^2} + \frac{1}{r}\frac{\partial C_{Alm}}{\partial r}\right] = k_1 C_{Alm} - \frac{k_1}{K_E}C_{Blm}^2 \qquad (19)$$

$$D_{Bm}\left[\frac{\partial^2 C_{Blm}}{\partial r^2} + \frac{1}{r}\frac{\partial C_{Blm}}{\partial r}\right] = -k_1 C_{Alm} + \frac{k_1}{K_E}C_{Blm}^2 \qquad (20)$$

A flux continuity equation at the boundary is assumed, giving the equations

$$r = r_t, \qquad D_{Am}\frac{\partial C_{Alm}}{\partial r}\Big|_{r_t} = D_{At}\frac{\partial C_{Alt}}{\partial r}\Big|_{r_t} \qquad (21)$$

$$r = r_t, \qquad D_{Bm}\frac{\partial C_{Blm}}{\partial r}\Big|_{r_t} = D_{Bt}\frac{\partial C_{Blt}}{\partial r}\Big|_{r_t} \qquad (22)$$

Equations 19 and 20 are solved along with the boundary conditions eqs 21 and 22 and then combined with the equations for the interior and the boundary conditions.

Absorption from a Gas Mixture. In gas absorption from a mixture, the gas-phase resistance has to be considered; an additional equation for the gas phase has to be solved. For CO_2 absorption in water, eq 4 is also valid for the gas flowing in the shell side. The shell-side gas velocity profile is given by eq 6. At the free surface $r = r_e$, the following boundary condition is valid:

$$\frac{\partial C_{igm}}{\partial r}(r_e,z) = 0 \qquad (23)$$

At two membrane interfaces the following conditions are valid:

$$r = r_t, \qquad C_{igm}|_{r_t} = \frac{C_{ild}|_{r_t}}{H} \qquad (24)$$

Table II. Parameters Used in the Absorption of SO_2 and CO_2 in Water

temp °C	solubility[a] of SO_2 (H_{iw}), mol/liter	diffusivity[a] of SO_2 ($10^5 D$), cm²/s	solubility[b] of CO_2 (H_{iw}), mol/L	diffusivity[c] of CO_2 ($10^5 D$), cm²/s	equilib[b] constant of SO_2 (K), mol/L
15	1.5420	1.34	0.045446	1.40	2.19
25	1.0559	1.76	0.3398	1.92	1.70

[a] Hikita et al. (1978). [b] Geankoplis (1972). [c] Majumdar et al. (1988).

$$r = r_0, \qquad C_{igm}|_{r_0} = C_{igs}|_{r_0} \qquad (25)$$

Flux continuity equations at the same boundaries are also valid, giving the equations

$$r = r_t, \qquad D_{im}\frac{\partial C_{igm}}{\partial r}\Big|_{r_t} = D_{it}\frac{\partial C_{ilt}}{\partial r}\Big|_{r_t} \qquad (26)$$

$$r = r_0, \qquad D_{im}\frac{\partial C_{igm}}{\partial r}\Big|_{r_0} = D_{is}\frac{\partial C_{igs}}{\partial r}\Big|_{r_0} \qquad (27)$$

Then, eq 4 is solved for the membrane phase with the above boundary conditions to give the gradients at $r = r_t$ and $r = r_0$, as

$$\frac{\partial C_{Alt}}{\partial r}\Big|_{r_t} = \left[C_{Ags}|_{r_0} - \frac{C_{Alt}|_{r_t}}{H}\right]\frac{D_{Am}}{D_{At}}\frac{1}{[\ln r_0 - \ln r_t]r_t} \qquad (28)$$

$$\frac{\partial C_{Ags}}{\partial r}\Big|_{r_0} = \left[C_{Ags}|_{r_0} - \frac{C_{Alt}|_{r_t}}{H}\right]\frac{D_{Am}}{D_{As}}\frac{1}{[\ln r_0 - \ln r_t]r_0} \qquad (29)$$

The equations for the shell and tube are combined with the above equations for the membrane inner and outer boundaries and solved simultaneously with the boundary conditions eqs 7 and 23 and the inlet conditions for CO_2 absorption. In the case of SO_2 absorption all the above equations and boundary conditions are valid except that the reaction term has to be taken into account; in addition similar relations are written for HSO_3^-. At the gas–liquid interface the formation of HSO_3^- is assumed to be zero (for details, see Karoor (1992)).

The above equations are solved using a finite difference scheme (Davis, 1984). The diffusion terms are discretized using the centered in space scheme, whereas the convection term is discretized using the upwind difference scheme. A downward difference scheme is used when the velocity in the shell side is in the opposite direction to that of the tube side. Using the method of lines, the above partial differential equations were reduced to a set of algebraic equations. These equations are tridiagonal in form as a result of the discretization method adopted. This set can now be easily solved using the Thomas algorithm (Karoor, 1992). In the case of SO_2 absorption the equation is solved for C_{Alt} (based on C_{Blt} values determined in the earlier iteration). The equations for C_{Blt} are solved using a similar approach; the nonlinear term in eqs 19 and 20 are pseudolinearized by representing C_{Blm}^2 and $C_{Blm}C_{Blm}^*$, where C_{Blm}^* is the value of C_{Blm} from the previous iteration. The solution procedure is continued till convergence is attained.

Results and Discussion

The results of countercurrent absorption of pure CO_2 and pure SO_2 in water flowing in the tube side of the hollow fiber modules are presented and discussed first. Performance of gas mixtures is provided later. Th values of the parameters used are given in Table II. The experimental results have been compared with the results btained from the numerical solution of the governing partial differential equations. Limited p rformance data have been provided also for shell-side water flow. Both experimental and
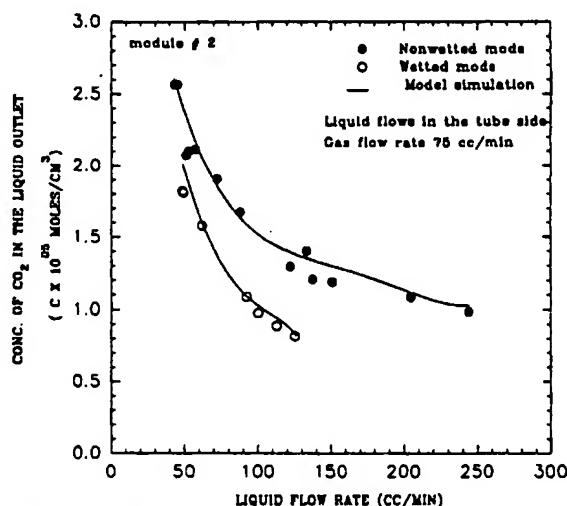

Figure 5. Comparison between wetted and nonwetted modes of operation for absorption of pure CO_2 in water.

model results have also been recast in the fashion of a plot of Sherwood number vs Graetz number. Besides the pure gas absorption experiments, the experimental results and the model simulations are discussed for cases where the feed gas is either a mixture of CO_2 (40%, 10%) in N_2 or a mixture of SO_2 (1%, 0.95%, 0.4%) in air. One or two or all three of the hollow fiber modules 2, 3, and 4 were used in these studies.

Figure 5 illustrates the variation of the liquid outlet concentration of CO_2 as a function of water flow rate in module 2. The gas flow rate was held constant at 75 cm³/min for all the runs shown in the figure as the liquid flow rate was varied. Data and numerical simulation results are presented for both nonwetted mode and wetted mode. It is clear that the liquid outlet CO_2 concentration in the wetted mode is lower than that in the nonwetted mode. This effect is more apparent as the liquid velocity is increased. Since the liquid boundary layer resistance decreases with increasing liquid velocity, the membrane resistance starts to control. By filling the pores with the absorbent liquid, the membrane-phase resistance is increased as the liquid offers additional resistance to the transport; this behavior highlights the fact that this is a liquid-phase-controlled process. Hence it would not be advantageous to operate under wetted-mode conditions for this particular system. Exactly the same trends were observed in the case of module 3. The theoretical curves shown in Figure 5 were obtained by solving eq 4 along with the boundary conditions. The theoretical predictions for these situations have a maximum deviation of 7% from the experimental results.

The effect of using a module with a higher contact area can be observed by using a greater number of fibers or increasing the length of the module. Figure 6 shows a plot of the concentration f CO_2 in the liquid outlet f r three different modules of varying surface area as a function of the liquid flow rate in the nonwetted m de. From Table I it is seen that module 2 has the maximum c ntact area followed by module 3 and then module 4. In the case of
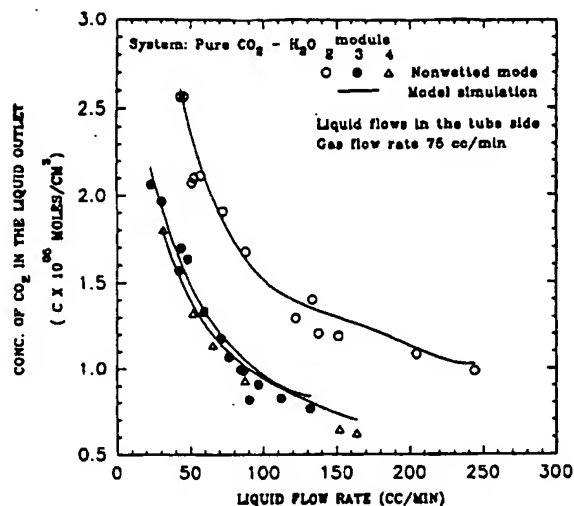
Figure 6. Comparison of concentration of CO_2 in the liquid outlet for modules of different surface area.
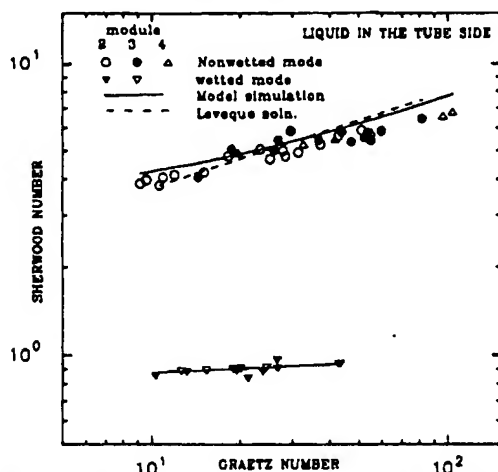

Figure 7. Sherwood number versus Graetz number variations for pure CO_2 absorption in water with different modules.

Figure 8. Effect of tortuosity on the CO_2 outlet concentration for module 2.

module 2, a higher amount of CO_2 in the liquid outlet is observed for the same liquid flow rate when compared with modules 3 and 4. Obviously using a longer module would require a higher pressure drop to achieve a given flow velocity. A maximum CO_2 removal of 76% was achieved in module 2 with a liquid flow rate of 244 cm³/min. The numerical model simulations describe these behavior quite well.

Figure 7 illustrates the same experimental results for modules 2, 3, and 4, but now as a plot of Sherwood number versus Graetz number, where Sherwood number is defined as $K_{Olm}(2r_t)/D_{At}$ for the nonwetted mode (for the wetted mode r_t is replaced by r_0) and Graetz number for the tube side is defined as $N_{Re}N_{Sc}\pi r_t/2L$. K_{Olm} is the logarithmic mean overall mass-transfer coefficient calculated by eq 1. A logarithmic mean driving force is used in the calculations as given by eq 2. An increase in Graetz number due to an increase in the the liquid flow rate increases the mass-transfer coefficient as expected. Another feature that can be observed is the effect of operating the module in the wetted mode. In the wetted mode the pores of the fiber are filled with th abs rbent liquid. This increases the resistance to mass transfer across the membrane p res, as a result of decreased gas diffusi n coefficient in the liquid phase. This effect is clearly sh wn in Figure 7 via a decrease in the Sherwood number by almost an rder f
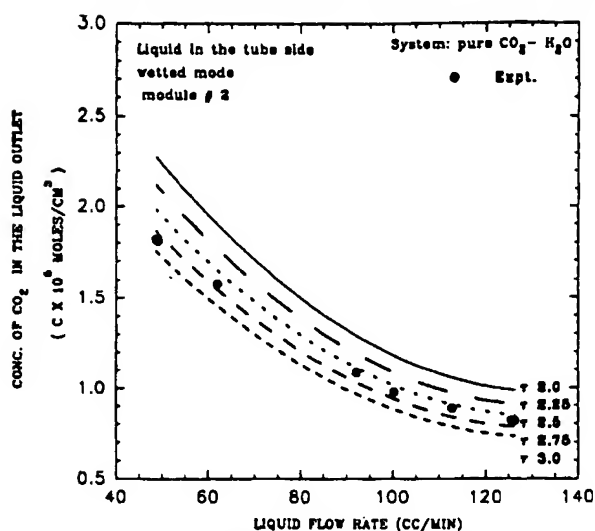
magnitude. As is evident from Figure 7, the effect of the wetted mode in module 3 was also observed to be similar. The extent of decrease in mass transfer in the wetted mode in module 3 is also comparable to that of module 2.

Figure 7 also illustrates the results obtained from the theoretical model for the nonwetted mode. The model results and the experimental observations show good agreement with a maximum deviation of about 11.5%. The Leveque solution (Leveque, 1928), also plotted in this figure, shows a reasonable agreement with the data. The Leveque solution results are somewhat higher at higher Graetz numbers.

In the wetted mode, an effective membrane diffusion coefficient was defined as $D_{Am} = D_{At}\epsilon/\tau$, where ϵ/τ was taken to be 0.4/2.5, from the experimentally measured values by Prasad and Sirkar (1988) for X-20 fibers with 240-μm inner diameter and 300-μm outer diameter. In the case of X-10 hollow fibers with 100-μm inside diameter an 150-μm outside diameter, the quantity ϵ/τ was taken to be 0.2/3.0.

Using this definition of effective diffusion coefficient and the values of ϵ/τ, the model discussed before for the wetted mode was solved numerically to obtain the results shown in Figure 7. The agreement between the model and experimental results is good with a maximum deviation of 7.5% for module 2. For module 3, Figure 7 shows that the agreement between the model results and experiments is again good with a maximum deviation of 12%. As discussed before, the length of module 2 is higher than that of module 3; also the number of fibers is greater in module 2 when compared to module 3. Thus, under similar operating flow rates, the Graetz number is lower for module 2 when compared to module 3, and it results in lower Sherwood numbers for module 2.

In Figure 8 the predicted CO_2 outlet concentration for module 2 in the wetted mode is plotted by allowing a maximum variation of ±20% in the tortuosity τ for X-20 fibers (2.5) used in the present study. As the tortuosity increases, the transfer of CO_2 into the liquid decreases since CO_2 has to diffuse through longer lengths of liquid. If the measured tortu sity is ±20% different from the value 2.5 used, then the maximum difference in the concentration is around 18% for the liquid flow rates and the system under study.

Figure 9 illustrates the results for module 3 when pure SO_2 flows in the shell side and water in the tube side. The
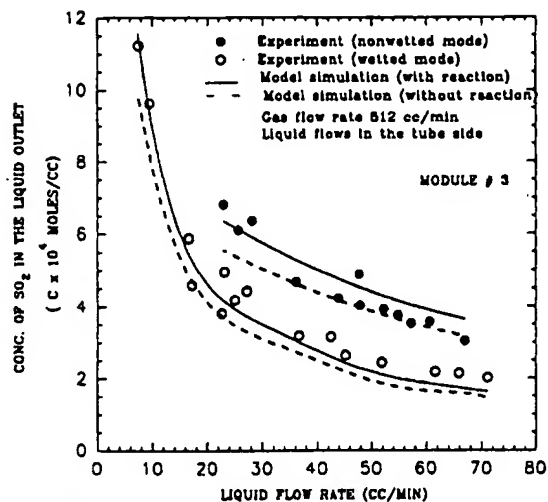
Figure 9. Absorption of pure SO_2 in water: concentration variation as a function of liquid flow rate for module 3.
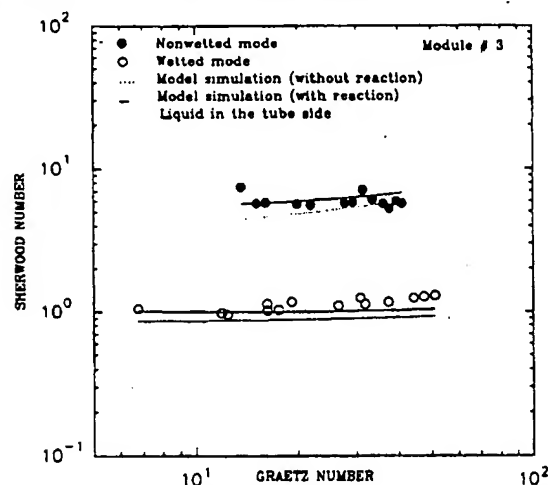

Figure 10. Sherwood number versus Graetz number for absorption of pure SO_2 in water.
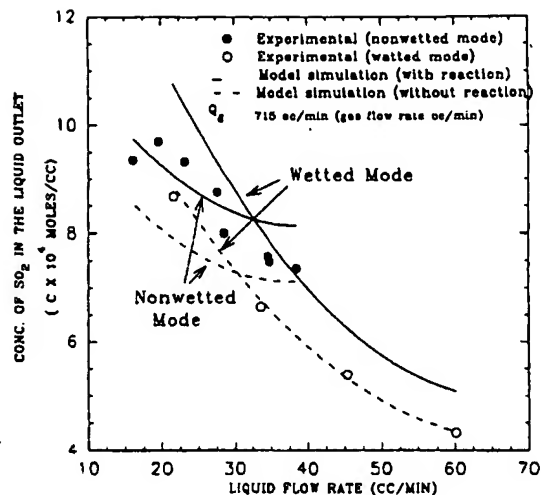

Figure 11. Absorption of pure SO_2 in water: liquid flowing in the tube side of module 2.
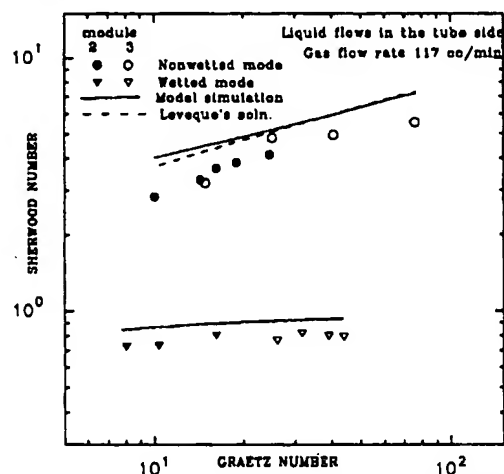
Figure 12. Sherwood number versus Graetz number for 10% CO_2 feed gas absorption in water.

experimental results have been indicated for both wetted and nonwetted modes; the wetted mode again offers higher resistance to mass transfer when compared to the non-w tted mode. Even though the solubility of SO_2 in water is high and there is a dissociation reaction, the reaction is not fast enough to make the liquid-filled-membrane resistance negligible. The theoretical predictions obtained by numerically solving the coupled differential equations explain the experimental results well with a maximum deviation of about 13%. The equations were also solved assuming that there is no reaction occurring between SO_2 and H_2O. It was found that there was a 10%–15% increase in predicted SO_2 concentration at the liquid outlet when the reaction term was included. Generally the latter approach describes the data much better especially in the wetted mode. It is worthwhile to note that a more rigorous analysis of SO_2 dissociation in water could have been carried out in view of the reaction being an instantaneous reversible one. However, the scatter in the data (Figure 9, nonwetted case) is considerable, and the enhancement due to SO_2 ionization in water is known to be around 10% (Danckwerts, 1970).

Figure 10 is a pl t of Sherwood number versus Graetz number for the absorption of pure SO_2 in water. The variation f Sherwood number with Graetz number is not very high in this case, due to the very high SO_2 s lubility

in water and the reaction that is occurring in the liquid phase. With a system having higher solubility or faster reaction rates, we may see a transition to gas-phase control (see Karoor (1992) for SO_2–Na_2SO_3 system).

Figure 11 shows the results for the same configuration with module 2 for pure SO_2 and water. At low liquid flow rates, when wetted and nonwetted modes of operations are considered, the difference in the concentration of SO_2 at the liquid outlet is small since the gas–liquid contact area is high and the liquid flow rate is low so that the liquid gets saturated before passing the whole length of the module.

So far, the cases studied utilized pure gas in the shell side; therefore the gas-phase resistance was negligible. Figure 12 shows the results for modules 2 and 3 when a feed gas containing 10% CO_2 in N_2 was flowing in the shell side and liquid was flowing countercurrently in the tube side. The results are presented as a plot of Sherwood number versus Graetz number. An increased resistance to mass transfer in the wetted mode is again apparent. The results of the model simulati ns show a maximum deviation f about 25% in the case of nonwetted mode. In the case f the wetted mode, the model seems to explain the experimental bservati ns within a maximum devi- ation f 18%. These deviations may have resulted from all f the gas n t coming into contact with the liquid in
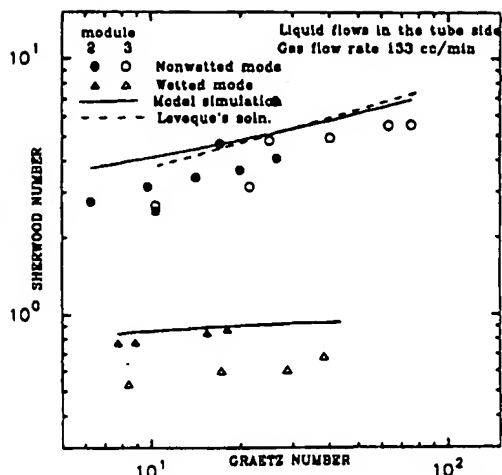
Figure 13. Sherwood number versus Graetz number for 40% CO_2 feed gas absorption in water.
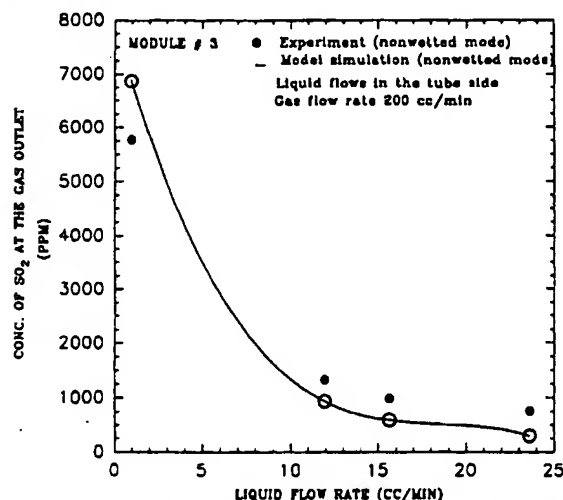

Figure 14. SO_2 absorption in water from 1% SO_2-air mixture in module 3.

Figure 15. Absorption of SO_2 from feed gases of pure SO_2 and SO_2-containing gas mixtures in water flowing in the shell side.

the modules which do not have high packing density. Similar trends were obtained in the case of the 40% CO_2-balance N_2 gas mixture (Figure 13); the maximum deviation in the nonwetted mode was around 25% in the case of module 2 and around 25% in the case of module 3. In the wetted mode, the deviation was 10% for module 2 and 35% in the case of module 3. This may be attributed to bypassing in the shell-side flow and to the fact that the packing fraction is lower in the case of module 3 when compared to module 2.

In these calculations the diffusion coefficient of the gas in the pores in the nonwetted mode was calculated from the transition regime of gas diffusion in porous media. Since r_p/λ was around 0.56, the diffusion of CO_2-N_2 in the pore was considered to be in the transition regime and not in the Knudsen regime. It was found that if the molecular diffusion coefficient was used there was no difference in the results as CO_2 absorption in water is liquid phase controlled.

Figure 14 identifies the concentration of SO_2 at the gas utlet for module 3 when 1% SO_2 (balance air) mixture was scrubbed using water in module 3. It is seen that, as the liquid flow rate increases, the concentration f SO_2 decreases, as expected. When the liquid flow rate was increased ab ve 40 cm^3/min, essentially n SO_2 was obs rved in the gas utlet. For module 2 at the same gas
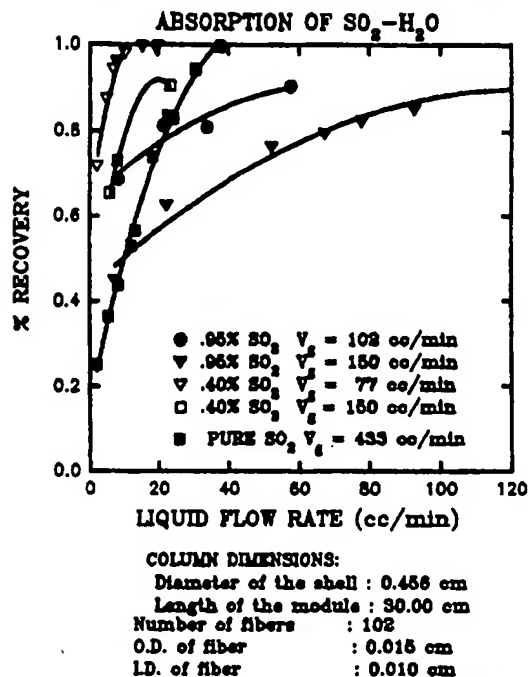
flow rate (200 cm^3/min), no SO_2 was observed experimentally at the gas outlet even at much lower liquid flow rates. This is because of the higher contacting area in the case of module 2 when compared with module 3. Thus it is observed that, with such small modules, it was possible to absorb all of the SO_2 using simple water as the absorbent.

For the systems CO_2-H_2O and SO_2-H_2O studied, the rate of absorption of the gas species scrubbed using the same module is much higher for SO_2 when compared to CO_2. There are several reasons for this: the solubility of SO_2 in water is 2 orders of magnitude higher than that of CO_2 and also the dissolution of SO_2 in water is accompanied by a reaction. Even though CO_2 reacts with water, the rate is orders of magnitude slower when compared to SO_2. Thus the absorption of SO_2 by water is enhanced by both the increased solubility and the chemical reaction.

It is useful now to identify the level of gas purification achieved using small hollow fibers modules having high surface areas. Usually most of the CO_2 and SO_2 were easily scrubbed out. In the case of SO_2, removal as high as 98% was achieved with a liquid flow rate of 38.46 cm^3/min and gas flow rate of 714.7 cm^3/min in the 30-cm-long, 0.49-cm-diameter module 2 from a pure SO_2 feed gas. When water is used as an absorbent, it is better to operate in a nonwetted mode.

Figure 15 shows the absorption of pure SO_2 and of SO_2 from SO_2-air mixtures when the absorbent liquid, water, flows in the shell side. Pure SO_2 removals as high as 99% were achieved with a liquid flow rate of about 40 cm^3/min in a 30-cm-long, 0.45-cm-diameter module 1 with a gas flow rate of about 433 cm^3/min. It is useful to know in this context that absorption of flue gases can be performed effectively using seawater (Radojevic and Tressider, 1992).

Considerable data were taken also when either pure CO_2 or CO_2-N_2 mixtures flowed on the tub side while water flowed countercurrently n th shell side (Karoor, 1992). The gas abs rption rates wer always significantly l wer in most f the systems studied c mpared to the tube-side liquid fl w cases due most likely to shell-side channeling. A much better gas absorpti n performance with shell-
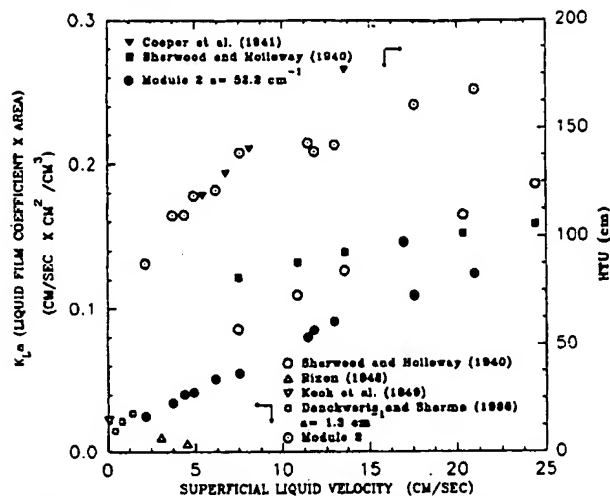
Figure 16. Comparison of K_La and HTU of a hollow fiber contactor to that of packed towers for CO_2 absorption in water.

Figure 17. Comparison of K_La and HTU of a hollow fiber contactor to that of packed towers for absorption of SO_2 in water.

side liquid flow was achieved using a crossflow module (Karoor, 1992). These results are not being reported here.

The pressure drop encountered in the gas-phase flow through the shell side was always very small for pure gas stream used here; mostly it was negligible. In a few cases the ΔPs encountered varied between 0.05 and 0.3 psi. When these gases flowed in the tube side, the ΔP was usually higher, in a few cases as much as 3–5 psi.

The absorption performance of a hollow fiber module needs to be compared with that of a conventional packed bed absorber. To this end, several experimental observations in a packed bed column for the CO_2–H_2O system reported in the literature are now compared to those of hollow fiber modules in Figure 16 using the data from the hollow fiber module 2 (dimensions of which are given in Table I). In this plot the equipment-average value of K_La obtained from the product of experimental K_{Olm} (eq 1) and a is plotted as a function of superficial liquid velocity (a is the interfacial gas–liquid contact area per unit volume). To obtain the superficial liquid velocity in a hollow fiber module in a manner equivalent to that defined for a packed bed, the following definition of superficial velocity is used for a hollow fiber contactor:

$$v_{sl} = \frac{F_1}{60(\text{empty cross-sectional area})} \quad (30)$$

where F_1 is the liquid flow rate in cm^3/min, empty cross-sectional area is defined as πr_s^2, and r_s is the shell inner radius. From the figure it is observed that, as the superficial velocity increases, the K_La also increases. Rixon (1948) studied the absorption of CO_2 in a commercial size plant where the column inner diameter was 27 in. and the packed height was 18 ft. The packing used was 1 1/2-in. × 1 1/2-in. stoneware. The K_La values obtained by them are quite low. Danckwerts and Sharma (1966) studied the absorption of CO_2 in water in a column of 18-in. diameter and the packing material 1 1/2-in. ceramic raschig rings. The values of K_La obtained by them were also low when compared to those in the hollow fiber module. In their case, the liquid film coefficients were very high but the area/volume was only 1.3 cm^2/cm^3, which resulted in low K_La values. Sherwood and Holloway (1940) used their O_2 desorption data and came up with general correlations f r calculating K_La and HTU for packed beds with vari us packing materials:

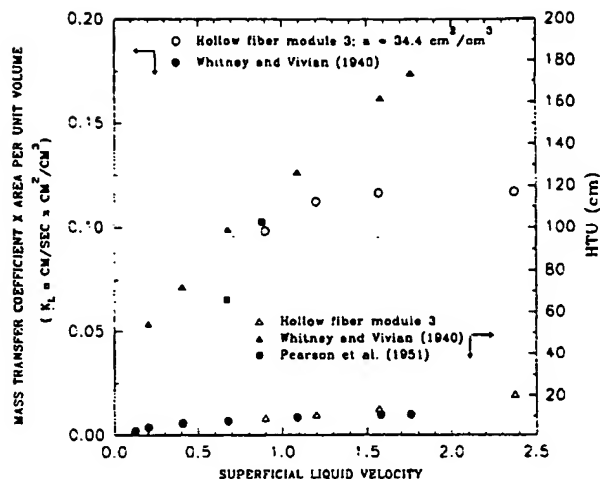$$\frac{K_La}{D_L} = a\left(\frac{L}{\mu_L}\right)^{1-n}\left(\frac{\mu_L}{\rho_L D_L}\right)^{1-s} \quad (31)$$

$$H_L = \text{HTU} = \frac{1}{\alpha}\left(\frac{L}{\mu_L}\right)^n\left(\frac{\mu_L}{\rho_L D_L}\right)^s \quad (32)$$

where K_La is the mass-transfer coefficient for liquid phase, h^{-1}; H_L is the height of an individual liquid-film transfer unit, ft; L is the liquid mass velocity, lb/(ft)^2(h); μ_L is the viscosity of the liquid, lb mass/(ft)(h); ρ_L is the density f the liquid, lb/ft^3; D_L is the diffusion coefficient for liquid phase, ft^2/h (approximately 6.6 × 10^{-5} ft^2/h for CO_2 at 18 °C); and α, n, and s are constants for various packings used. The above equations provide general estimates of K_La and HTU values at low liquid flow rates. The above equations can also be used for absorption of CO_2 as the gas-film resistance is generally neglected. As seen in Figure 16, the K_La values from such an equation are always smaller than those obtained in the hollow fiber contactor. Also most of the data for packed beds are available for low liquid flow rates; at higher liquid flow rates there may be flooding or loading. Thus, even with a simple absorbent liquid used in these experiments, a remarkably higher amount of removal was achieved with relatively small modules and flow velocities. The potential for increased removal is enormous with the application of reactive absorbents and appropriate operating conditions.

Figure 16 shows also the HTU variation as a function of the superficial liquid velocity. The HTU in the case of a hollow fiber is given as

$$\text{HTU} = \frac{v_{sL}}{K_La} \quad (33)$$

In the figure the data obtained by Cooper et al. (1941) in a 2-in. × 2 1/16-in. steel raschig ring column show the highest HTU for a given superficial velocity. The HTU given by eq 32 (Sherwood and Holloway, 1940) is also plotted. As seen in the figure, the equation still yields higher HTU when compared to that for a hollow fiber contactor. The difference is especially large at lower superficial velocities.

Figure 17 compares the K_La values for hollow fiber module 3 to those of packed towers for SO_2 absorption in water. The K_La is plotted as a function of the superficial velocity. The K_La increases as the superficial velocity increases. Whitney and Vivian (1949) studied the absorption f SO_2 in water in a 8-in.-diameter tower using 1-in. ceramic packing; as bserved from the figure the K_La btained by them were 1 w. At a superficial velocity of 1.5 cm/s, the K_La obtained in a hollow fiber module is

around 10 times higher than that obtained in a packed tower. Figure 17 compares also the HTU of hollow fiber module 2 to that of packed towers. The data obtained by Whitney and Vivian (1949) and Pearson et al. (1951) are plotted as a function of the superficial velocity. As observed from the figure, very low HTU values were obtain d when a holl w fiber module was used f r gas-liquid contacting when compared to th packed towers.

Conclusions

For CO₂ absorption in water and SO₂ absorption in water in hydrophobic microporous hollow fiber modules, both liquid and gas flow rates were controlled independently, and there were no operational problems in either wetted or nonwetted modes of operation. For CO₂ absorption in water, the wetted mode of operation offers considerably higher resistance to mass transfer when compared to the nonwetted mode of operation. It is a liquid-phase-controlled process; thus filling the membrane pores with water increases the resistance to mass transfer. Increasing the contact area in a given module or the packing fraction for a given fiber size increases the CO₂ removal capacity. The contact area in a hollow fiber device can be increased by increasing the number of fibers without any substantial increase in the physical size of the contacting device. When the absorbent liquid, water, flows in the tube side, simulation results from a model based on first principles are in good agreement with experimental observations. The Leveque solution also agrees well with the experimental results. The experimentally obtained K_La values for the contactors are considerably larger than those for packed towers. Even though the mass-transfer coefficients obtained for hollow fiber modules in this study are similar to or lower than the values reported for packed beds in the literature, the contact area per unit equipment volume in the case of hollow fiber devices is many times higher than that for packed towers. Therefore, at a superficial liquid velocity of 1.25 cm/s, the K_La value was 5 times higher than that for a conventional packed tower. As the liquid flow rate increases, the difference in the K_La values is decreased. At higher flow rates, there are operational problems in packed tower like flooding and loading; there is no such problem in a hollow fiber module as long as the correct phase pressure conditions are maintained. The HTU in a hollow fiber module is several times lower than that in a packed tower operating under similar flow conditions.

For the absorption of SO₂ in pure water in a microporous hollow fiber contactor, the following conclusions are relevant. The K_La value for a hollow fiber contactor was about 10 times higher than that for conventional packed towers for a superficial liquid velocity of 1.5 cm/s. The HTUs obtained were also about 10 times lower than those obtained for a packed tower for SO₂ absorption in water. Thus efficient contacting is achieved in the case of a hollow fiber when compared to conventional contactors. In the case of SO₂ absorption in water, removal rates as high as 99% were attained in module 1 (a ¹/₄-in. tube containing 102 X-10 fibers, 30 cm long). Thus, even in a small module high removal rates were attained, proving the efficiency of the contactor. Incorporation of SO₂ dissociation reaction in pure water predicts 10%–15% higher SO₂ concentration in the liquid outlet. The wetted mode of operation with pure water as absorbent offers somewhat higher resistance when compared with the nonwetted mode of operation. Thus it is advantageous to perate the module in the nonwetted mode. Higher contact areas per unit module v lume provide higher SO₂ rem val efficiencies. The

model simulations are in good agreement with the experimental observations for cases where the absorbent liquid fl wed in the tube side.

Nomenclature

a = gas–liquid interfacial area/contactor volume (cm⁻¹)

A_T = mass-transfer area based on surface area of gas–liquid contact (cm²)

C_{ijk} = concentration of species i in the phase j (j = g, for gas, and j = l, for liquid) and in region k (k = m, for fiber wall pore, k = s, for shell side, and k = t, for fiber bore) (mol/cm³)

C_{Aw} = concentration of species A in liquid at the gas–liquid interface at the membrane wall (mol/cm³)

C_{Bw} = concentration of species B in liquid at the gas–liquid interface at the membrane wall (mol/cm³)

$C_{g\ in}$ = concentration of the absorbed gas species at the gas stream inlet (mol/cm³)

$C_{g\ out}$ = concentration of the absorbed gas species at the gas stream outlet (mol/cm³)

C_{ig} = concentration of species i in the gas phase at the gas–liquid interface (mol/cm³)

C_{il} = concentration of species i in the liquid phase at the gas–liquid interface (mol/cm³)

$C_{l\ out}$ = concentration of CO₂ or SO₂ in liquid outlet (mol/cm³)

ΔC_{lm} = logarithmic mean concentration difference of CO₂ or SO₂ (mol/cm³)

D_{Bl} = diffusion coefficient of species B in the liquid phase (cm²/s)

D_{ik} = diffusion coefficient of species i in region k (k = m, for fiber wall pore, k = s, for shell side, and k = t, for tube side) (cm²/sec)

$F_{g\ in}$ = gas flow rate at module inlet (cm³/min)

$F_{g\ out}$ = gas flow rate at module outlet (cm³/min)

H = dimensionless Henry's constant as defined by eq 3

k_1 = forward rate constant for SO₂ ionization (s⁻¹)

K_E = equilibrium constant of a chemical reaction

K_{Olm}, K_L = overall mass-transfer coefficient (cm/s)

L = effective length of the module, cm

N_f = total number of fibers in the hollow fiber module

N_{Gz} = Graetz number, $\pi r_i N_{Re} N_{Sc}/2L$

N_{Re} = Reynolds number, $2r_i v_{rt} \rho/\mu$

N_{Sc} = Schmidt number, $\mu/\rho D_{At}$

N_{Sh} = Sherwood number, $K_{Olm}(2r_i)/D_{At}$

P_g, P_{gu} = gas-phase pressure (psig)

P_{aq} = liquid-phase pressure (psig)

r = radial coordinate position (cm)

r_e = free surface radius (see eq 6) (cm)

r_i = molar production rate of species i by reaction per unit volume (mol/(cm³·s))

r_0, r_t = outer radius and inner radius of the fiber (cm)

r_p, r_s = pore diameter, shell radius (cm)

R_{gas} = gas constant (atm·cm³/(mol K))

T_R = room temperature (°C)

v_{rs}, v_{rt} = shell side and tube side velocity (cm/s)

V_l = liquid flow rate (cm³/min)

Greek Letters

ϵ = packing fraction

μ_j = viscosity of the fluid in the shell side (gm/(cm·s))

λ = mean free path (cm)

ρ = density (g/cm³)

τ = tortuosity of the membrane pore

Subscripts

A, B = species CO_2 and HSO_3^-, respectively

i = component involved

j = phase involved (j = g, gas, or j = l, liquid)

k = location of the species (k = m, for fiber wall pore, k = s, for shell side, and k = t for tube side)

Literature Cited

AWWA. *Standard Methods for the Examination of Water and Wastewater*, American Water Works Association: New York, 1965.

Betz. *Betz Handbook of Industrial Water Conditioning*; Betz: Philadelphia, 1962.

Bhave, R. R.; Sirkar, K. K. Gas Permeation and Separation by Aqueous Membranes Immobilized Across the Whole Thickness or in a Thin Section of Hydrophobic Microporous Celgard Films. *J. Membr. Sci.* 1986, *27*, 41–61.

Bhave, R. R.; Sirkar, K. K. Gas Permeation and Separation with Aqueous Membranes Immobilized in Microporous Hydrophobic Hollow Fibers. In *Liquid Membranes Theory and Applications*; Noble, R. D., Way, J. D., Eds.; ACS Symposium Series 347; American Chemical Society: Washington, DC, 1987; Chapter 10, pp 138–151.

Cooper, C. M.; Christ, R. J.; Peery, L. C. Packed Tower Performance at High Liquor Rates. *Trans. Am. Inst. Chem. Eng.* 1941, *37*, 979.

Danckwerts, P. V. *Gas-Liquid Reactions*; McGraw Hill: New York, 1970; p 129.

Danckwerts, P. V.; Sharma, M. M. The Absorption of Carbon Dioxide into Solutions of Alkalis and Amines. (with some notes on hydrogen sulphide and carbonyl sulphide). *Chem. Eng.* 1966, CE244–CE279.

Davis, M. E. *Numerical Methods and Modeling for Chemical Engineer*; Wiley: New York, 1984.

Esato, K.; Eiseman, B. Experimental Evaluation of Gore-Tex Membrane Oxygenator. *J. Thorac. Cardiovas. Surg.* 1975, *69* (5), 690–697.

Geankoplis, J. C. *Mass Transport Phenomena*; Ohio State University Bookstores: Columbus, OH, 1972.

Gill, W. N.; Bansal, B. Hollow Fiber Reverse Osmosis Systems Analysis and Design. *AIChE J.* 1973, *19* (4), 823–831.

Happel, J. Viscous Flow Relative to Arrays of Cylinders. *AIChE J.* 1959, *5* (2), 174–177.

Hikita, H.; Asai, S.; Nose, H. Absorption of SO_2 into Water. *AIChE J.* 1978, *24* (1), 147–149.

Karoor, S. Gas Absorption Using Microporous Hollow Fiber Membranes. Ph.D. Dissertation, Stevens Institute of Technology, Hoboken, NJ, 1992.

Keller, K. H.; Stein, T. R. A Two Dimensional Analysis of Porous Membrane Transport. *Math. Biosci.* 1967, *1*, 421–437.

Kim, B. S.; Harriott, P. Critical Entry Pressure for Liquids in Hydrophobic Membranes. *J. Colloid Interface Sci.* 1987, *115*, 1.

Koch, Jr.; Stutzman, L. F.; Blum, H. A.; Hutchings, L. E. Liquid Transfer Coefficient for CO_2-air-H_2O System. *Chem. Eng. Prog.* 1949, *45*, 677–682.

Leveque, J. Les Lois de la Transmission de Chaleur par Convection. *Ann. Mines* 1928, *13*, 201, 305, 381.

Majumdar, S.; Guha, A. K.; Sirkar, K. K. A New Liquid Membrane Technique for Gas Separation. *AIChE J.* 1988, *34* (7), 1135–1145.

Ogundiran, O. S.; Varanasi, S.; LeBlanc, S. E. A Novel Gas Desulfurization Process Using Hollow Fiber Membranes. Presented at the Air Pollution Control Association Meeting, Cleveland, OH, October 1988.

Ogundiran, O. S.; LeBlanc, S. E.; Varanasi, S. Membrane Contactors for SO_2 Removal from Flue Gases. Presented at the Pittsburgh Coal Conference, Pittsburgh, PA, September, 1989.

Pearson, D. A.; Lundberg, L. A.; Frank, B. W.; Joseph, L. M. Absorption on a Semi-Works Scale. Absorption of Sulfur Dioxide in Water in Packed Tower. *Chem. Eng. Prog.* 1951, *47* (5), 257–264.

Prasad, R.; Sirkar, K. K. Dispersion-Free Solvent Extraction with Microporous Hollow-Fiber Modules. *AIChE J.* 1988, *34* (2), 177–187.

Qi, Zhang; Cussler, E. L. Microporous Hollow Fibers for Gas Absorption. I. Mass Transfer in the Liquid. *J. Membr. Sci.* 1985a, *23*, 321–332.

Qi, Zhang; Cussler, E. L. Microporous Hollow Fibers for Gas Absorption. II. Mass Transfer Across the Membrane. *J. Membr. Sci.* 1985b, *23*, 333–345.

Radojevic, M.; Tressider, D. A. Absorption of Flue Gas by Water. *Nature* 1992, *356* (April 2), 391.

Rixon, F. F. The Absorption of CO_2 in and Desorption From Water Using Packed Towers. *Trans. Inst. Chem. Eng. (London)* 1948, *26*, 119–130.

Roberts, D. L. Sulfur Dioxide Transport through Aqueous Solutions. Ph.D. Thesis, California Institute of Technology, Pasadena, CA, 1979.

Seinfeld, J. H. *Lectures in Atmospheric Chemistry*; AIChE Monograph Series 76; American Institute of Chemical Engineers: New York, 1980.

Sengupta, A.; Raghuraman, B.; Sirkar, K. K. Liquid Membranes for Flue Gas Desulfurization. *J. Membr. Sci.* 1990, *51*, 105–126.

Sherwood, T. K.; Holloway, F. A. L. Performance of Packed Tower—Experimental Studies of Absorption and Desorption. *Trans. Am. Inst. Chem. Eng.* 1940, *36* (Feb 25), 21–37.

Sirkar, K. K. Other New Membrane Processes. In *Membrane Handbook*; Ho, W. S. Winston, Sirkar, K. K., Eds.; Van Nostrand Reinhold: New York, 1992; pp 885–899.

Skelland, A. H. P. *Diffusional Mass Transfer*; Wiley: New York, 1974; p 162.

Snell, F. D.; Hitton, C. L. *Encyclopedia of Industrial Chemical Analysis*; Interscience: New York, 1966.

Tsuji, T.; Suma, K.; Tanishita, K.; Fukazawa, Z.; Kanno, M.; Hasegawa, H.; Takahashi, A. Development and Clinical Evaluation of Hollow Fiber Membrane Oxygenator. *Trans. Am. Soc. Artif. Intern. Organs.* 1981, *27*, 280–284.

Vinograd, J. R.; McBain, J. W. Diffusion of Electrolytes and of the Ions in their Mixtures. *J. Am. Chem. Soc.* 1941, *63*, 2008–2015.

Wang, J. C.; Himmelblau, D. M. A Kinetic Study of Sulfur Dioxide in Aqueous Solution with Radioactive Tracers. *AIChE J.* 1964, *10* (4), 574–580.

Whitney, R. P.; Vivian, J. E. Absorption of Sulfur Dioxide in Water. *Chem. Eng. Prog.* 1949, *45* (5), 323–337.

Yang, M. C.; Cussler, E. L. Designing Hollow-Fiber Contactors. *AIChE J.* 1986, *32*, 1910–1916.